Identification of 50S Components Neighboring 23S rRNA Nucleotides A2448 and U2604 within the Peptidyl Transferase Center of *Escherichia coli* Ribosomes†

Serguei N. Vladimirov, Zhanna Druzina, Ruo Wang,‡ and Barry S. Cooperman*

Department of Chemistry, University of Pennsylvania, Philadelphia, PA 19104-6323

Received August 10, 1999; Revised Manuscript Received October 20, 1999

ABSTRACT: The 23S rRNA nucleotides 2604−12 and 2448−58 fall within the central loop of domain V, which forms a major part of the peptidyl transferase center of the ribosome. We report the synthesis of radioactive, photolabile 2′-O-methyloligoRNAs, PHONTs **1** and **2**, complementary to these nucleotides and their exploitation in identifying 50S ribosomal subunit components neighboring their target sites. Photolysis of the 50S complex with PHONT **1**, complementary to nts 2604−12, leads to target site-specific photoincorporation into protein L2 and 23S rRNA nucleotides A886, A1918, A1919, G1922-C1924, U2563, U2586, and C2601. Photolysis of the 50S complex with PHONT **2**, complementary to nts 2448−58, leads to target site-specific probe photoincorporation into proteins L2, L3, one or more of proteins L17, L18, L21, and of proteins L9, L15, L16, and 23S rRNA nucleotides C2456 and ψ2457. Chemical footprinting studies show that 2′-O-methyloligoRNA binding causes little distortion of the peptidyl transferase center but do provide suggestive evidence for the location of flexible regions within 23S rRNA. The significance of these results for the structure of the peptidyl transferase center is considered.

With the recent publications of X-ray structures of the 70S ribosome (7.8 Å resolution) (*1*), 30S subunit (5.5 Å resolution (*2*)), and 50S subunit (5.0 Å resolution (*3*)), prospects that ribosome function will be explainable in terms of ribosome structure at a molecular level have never been brighter. At present, a major difficulty in determining ribosome structure remains the correct placement of ribosomal components: the accurate tracing of the RNA backbone and the orientation of ribosomal proteins alongside that backbone.

We have been using radioactive photolabile oligonucleotide probes (PHONTs[1]) targeted toward functionally important sites of 23S rRNA to identify proteins and individual nucleotides site-specifically photolabeled from these sites (*4*−*8*). Such information is important for the related processes of detailed model building and structure determination.

In the present work, we target *Escherichia coli* 23S rRNA nucleotides 2604−12 and 2448−58. These nucleotides fall within the central loop of domain V of 23S rRNA, which has been strongly implicated in peptidyl transferase (PT) activity (*9*−*12*). Mutations of nucleotides within the loop give rise either to losses in PT activity (*13*) or to resistance to antibiotic inhibitors of PT activity (*14*). In addition, sites within the loop can be photocrosslinked both to photolabile derivatives of aminoacyl tRNAs (*11*) and puromycin (*15*) and are protected from chemical modification by A-site and P-site bound tRNAs and by antibiotic inhibitors of PT activity (*16*, *17*).

Below, we report results using two 23S rRNA-directed PHONTs, 2′-O-methyloligoRNA-2612−04-C7-Az, **1**, and 2′-O-methyloligoRNA-2458−48-C7-Az, **2** (Figure 1). Both PHONTs are 2′-O-methyl-oligoribonucleotides, complementary to the nucleotides indicated and contain a *p*-azidobenzoyl group attached via an amino group placed at the 3′-end of the molecule. They permit us to identify ribosomal components within 25 Å of 23S rRNA nucleotides U2604 and A2448.

EXPERIMENTAL SECTION

Except as specified below, materials were obtained and methods were performed as described elsewhere (*4*−*8*, *18*).

Materials. *Synthesis and Purification of Oligonucleotides*. The following oligonucleotides were synthesized using phosphoramidite chemistry as previously described (mismatches with the target sequence are in italics). Targeted to 23S rRNA: cDNA-2612-04, 2′-O-methyloligoRNA-2612−04 (sequence for both, 5′-GGGACCGAA-3′), mismatched 2′-O-methyloligoRNA-2612-04 (MM-2′-O-methyloligoRNA-2612-04, sequence 5′-G*CCU*CCGAA-3′), 2′-O-methyloligoRNA-2458-48 (sequence 5′-CAGCCUGUUAU-3′), MM-2′-O-methyloligoRNA-2458-48 (sequence 5′-CAG*GGACA*-UAU-3′), 2′-O-methyloligoRNA-2258-53/2(S)-48, which contains a phosphorothioate group bridging the sixth and the seventh nucleotides (sequence 5′-GACCGC(S)CCCAG-3′), MM-2′-O-methyloligoRNA-2258-48 (sequence 5′-GAC*A*-

† This work was supported by NIH grant GM-53416.

* Corresponding author. Telephone: 215-898-6330. Fax: 215-898-2037. E-mail: cooprman@pobox.upenn.edu.

‡ Present address: Schering-Plough Research Inst., 2015 Galloping Hill Rd., K-15-3-3545, Kenilworth, New Jersey 07033-0539.

[1] Abbreviations used are: AMV, avian myeloblastosis virus; bp, base pair; CC, induced chemical cleavage; EXL, electrophilic cross-linking; FP, chemical footprinting; MM, mismatched; nt, nucleotide; PAGE, polyacrylamide gel electrophoresis; PHONT, photolabile oligonucleotide probe, PT, peptidyl transferase; PTC, peptidyl transferase center; ϕXL, photo cross-linking; RP-HPLC, reverse phase high performance liquid chromatography; TBE, 89 mM Tris-borate (pH 8.3), 2 mM EDTA; TFA, trifluoroacetic acid; $TKM_{0.5}$, 50 mM Tris-HCl (pH 7.6), 50 mM KCl, 0.5 mM $MgCl_2$; TKM_{10}, 50 mM Tris-HCl (pH 7.6), 50 mM KCl, 10 mM $MgCl_2$; TND, 20 mM Tris-HCl (pH 7.9), 100 mM NaCl, 1 mM dithiothreitol; TP50, total protein from 50S subunits.

10.1021/bi991866o CCC: $19.00
Published on Web 12/11/1999

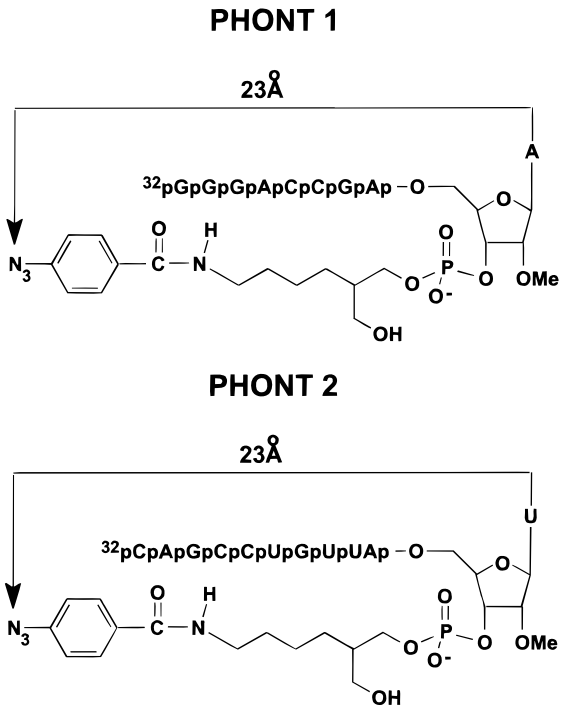

FIGURE 1: PHONTs **1** (2′-O-methyloligoRNA-p*2612-04-C7-Az) and **2** (2′-O-methyloligoRNA-p*2458-48-C7-Az). The distance between the photogenerated nitrene and either the N^6 of the adenosine complementary to U2604 (PHONT **1**) or the O^4 of the uracil complementary to A2448 (PHONT **2**) is 23 Å, as determined by molecular modeling with Quanta4.1 (Molecular Simulations, Inc.).

*CAA*CCAG-3′), 2′-O-methyloligoRNA-782-72 (sequence 5′-UUCACCCCCAG-3′). *Targeted to 16S rRNA*: cDNA-1531-22 (sequence 5′-TCCAACCGCA), and 2′-O-methyloligoRNA-1405-02/1(S)-1397, which contains a phosphorothioate group bridging the fourth and the fifth nucleotides (sequence 5′-CGGG(S)CGGUG-3′).

Both 2′-O-methyloligoRNA-2612-04-C7-Az, PHONT **1**, and 2′-O-methyloligoRNA-2458-48-C7-Az, PHONT **2** (Figure 1), were synthesized as follows. 3′-Amino-modifier C7 CPG [(1-dimethoxytrityloxy-3-fluorenylmethoxycarbonylamino-hexan-2-methylsuccinoyl) long-chain alkylamino-CPG] was used to generate a 2′-O-methyloligoRNA derivatized at its 3′-end with a primary amine, according to the protocol supplied by Glen Research (Sterling, VA). After deprotection and RP-HPLC purification, the 3′-amino group was reacted with *N*-hydroxysuccinimidyl-4-azidobenzoate to yield PHONT **1** or **2**, using a procedure described earlier (*4*). PHONTs **1** and **2** were each purified away from residual underivatized material by RP-HPLC on a C18 reverse-phase column using a linear 5−40% acetonitrile gradient in 0.1 M triethylamine/acetate (pH 7.6), and each was radiolabeled at its 5′-end with [γ-^{32}P]-ATP using polynucleotide kinase, producing 2′-O-methyloligoRNA-p*2612-04-C7-Az and 2′-O-methyloligoRNA-p*2458-48-C7-Az. cDNA 2612-04, labeled at its 5′-end, p*2612-04, was prepared similarly. Radiolabeled oligonucleotides were purified using Sep-pak (C-18) cartridges.

Methods. *Filter Binding Assay*. 50S subunits (12.5−15 pmol in 25 μL) were incubated with varying amounts of ^{32}P-labeled nucleotides using a protocol (incubation in $TKM_{0.5}$ followed by TKM_{10}), essentially identical to that described below for the preparation of photoincorporation samples. This two step incubation procedure afforded higher levels of binding than those found if binding was conducted only with incubation in TKM_{10}. HAWP 0.45 μm filters (Millipore) were prewashed with 5 mL of TKM_{10}. The reaction mixtures were diluted with 0.5 mL of cold TKM_{10} and filtered through nitrocellulose filters, followed by three 1 mL washes with TKM_{10}. The amount of filter-bound oligonucleotide was determined by liquid scintillation counting of the dried filters. Binding measurements were performed in triplicate.

Photoincorporation of [^{32}*P*]*-labeled PHONTs* ***1*** *and* ***2*** *into 50S Subunits*. 50S subunits (typically 300 pmol), preactivated by heating with 10 mM Mg^{2+} at 37 °C for 20 min, were combined in $TKM_{0.5}$ with photolabile probe (typically 20 pmol) in the absence or presence of either competing complementary 2′-O-methyloligoRNA or of mismatched 2′-O-methyloligoRNA (typically at a 10-fold excess over subunits) in a total volume of 150 μL. The photolysis mix was incubated for 5 min at 37 °C and then for 10 min on ice. The $MgCl_2$ concentration was then increased to 10 mM and the mixture was incubated for 5 min at 37 °C and kept on ice for 30 min. 50S subunits treated in this manner sediment at the normal 50S position in sucrose gradients (*6*). Photolysis was performed for 4 min at 4 °C in a Rayonet RPR Photochemical Reactor equipped with RPR-3000 Å phosphor-coated low-pressure Hg lamps (Southern New England Ultraviolet Co., Hamden, CT). Immediately after photolysis, azide-derived radicals were quenched by the addition of 5 μL 2 M 2-mercaptoethanol. The photolysis mix was transferred to Eppendorf tubes and subunits were precipitated with two volumes of 9:1 (v/v) ethanol/2-mercaptoethanol. Subunits were pelleted from the ethanol/2-mercaptoethanol by centrifugation for 15 min at 4 °C, washed with 200 μL 70% EtOH, repelleted, dried under a nitrogen stream and dissolved in TKM_{10}.

Extraction of rRNA from Acetic Acid Insoluble Pellets. To isolate rRNA and proteins from the same photolabeled sample, rRNA was prepared from the pellet that remains following extraction of proteins with 67% acetic acid. The pellet was dissolved in 200 μL water and sodium acetate was added to a final concentration of 0.1 M. rRNA was extracted with equal volumes of phenol (twice), phenol/chloroform (1:1), and chloroform, and was precipitated with 2.5 volumes of EtOH (−20 °C, 1 h). The pellet obtained by centrifugation was washed with 70% EtOH, dried under N_2, dissolved in 1 mM EDTA, and stored at −80 °C.

Chemical Footprinting. The procedures utilized followed Moazed et al. (*19*) as modified in (*8*). In experiments measuring the effects of added oligonucleotides on chemical footprinting, the oligonucleotide/50S molar ratio was ten.

RESULTS

Noncovalent Binding of Oligonucleotides to the 50S Subunit. Noncovalent binding of oligonucleotides to the 50S subunit was determined using a Millipore filter binding assay (Figure 2). 2′−O-methyloligoRNA-p*2612-04 binds much more tightly than the corresponding cDNA, consistent with results showing that 2′-OMe oligoribonucleotides form far more stable duplexes with RNA strands than their deoxy counterparts (*20*); 2′-O-methyloligoRNA-p*2612−04 also binds somewhat more tightly than PHONT **2**. Both of these oligonucleotides show biphasic binding, with a tight binding

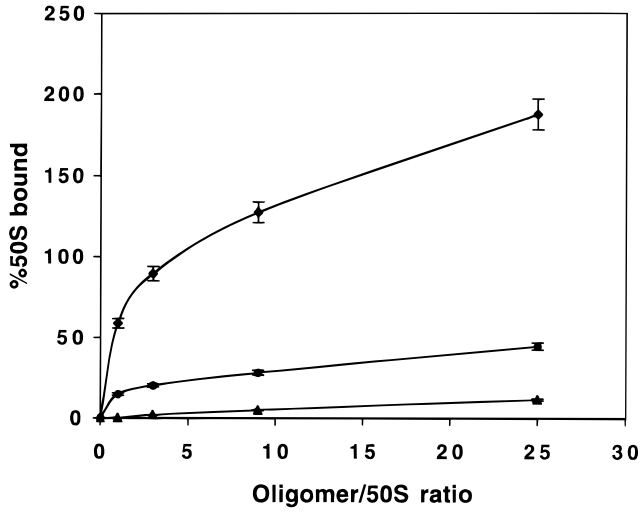

FIGURE 2: Noncovalent binding of oligonucleotides to 50S subunits. (◆) 2′-O-methyloligoRNA-p*2612-04;(▲)cDNA-p*2612-04; (●) 2′-O-methyloligoRNA-p*2458-48-C7-Az.

stoichiometry of ~ 0.9 for 2′-OMe-p*2612-04 vs ~0.17 for PHONT **2**. In other experiments, the shorter oligonucleotide 2′-O-methyloligoRNA-2455-48 was found to bind only weakly to 50S subunits, with levels not exceeding 3% of 50S subunits at oligonucleotide/50S ratios as high as 30 (data not shown).

Evidence that nts 2604−12 are available for probe binding, at least in 23S rRNA, was provided by the ~300 nt fragment that was generated on digestion of 23S rRNA with RNase-H in the presence of a hybrid DNA/2′O-Me oligonucleotide probe complementary to 2604−12 (data not shown). This hybrid oligonucleotide contained four consecutive deoxynucleotides in the interior positions 2609−2606, thus generating an RNase-H site on binding to 23S rRNA (*21*). The exterior positions were 2′-O-Me nucleotides.

*Photo-cross-linking of PHONTs **1** and **2** to 50S RNA and Proteins*. Except as otherwise indicated, photo-cross-linking experiments were conducted on samples in which 50S subunits were in stoichiometric excess over PHONT (typically 15-fold) in order to maximize incorporation from higher affinity binding sites (Figure 2). The amount of PHONT incorporated into the RNA fraction of 50S subunits photolyzed either in the absence of competing complementary 2′-O-methyloligoRNA, or in the presence of the mismatched 2′-O-methyloligoRNA, was consistently higher than in the control photolysis with preirradiated PHONT or on photolysis in the presence of competing complementary 2′-O-methyloligoRNA (Table 1). For PHONTs **1** and **2**, 10−20 % of the PHONT was site-specifically photoincorporated into 50S rRNA, measured as the difference in photoincorporation in the absence and presence of competing 2′-O-methyloligoRNA. The corresponding photoincorporation into TP50, as estimated from total radioactivity coeluting with 50S protein on RP-HPLC analysis, was lower and much less site-specific. This pattern of higher site-specificity in RNA vs protein labeling is typical of our results with photolabile oligonucleotides (*4*−*8*, *18*). Little if any photoincorporation into RNA or protein was observed on irradiation of either ^{32}P-2′-O-methyloligoRNA 2612-04 or ^{32}P-2′-O-methyloligoRNA 2458-48 with 50S subunits, demonstrating the aryl azide-dependence of the photoincorporation process.

For photoincorporation into both limited regions of RNA and single 50S proteins, site-specific photoincorporation of PHONT **1** or **2** was demonstrated by a large reduction of photoincorporation in the presence of competing complementary 2′-O-methyloligoRNA but not in the presence of the mismatched 2′-O-methyloligoRNA (vide infra).

Localization of Specifically Labeled Regions in 50S rRNA. Partial localization of photocrosslinking sites was achieved by RNase-H cleavage of the labeled 23S rRNA hybridized with various oligo cDNAs. The fragments excised by RNase-H were analyzed by urea-PAGE and autoradiography. The apparent sizes of labeled fragments, as determined by comparison with RNA size markers, are typically 10−20 nts larger than would be expected for calculated unlabeled fragments, due to both the size of photoincorporated probe itself (9 or 11 nts) and the multiple sites of RNase-H hydrolysis within a given cDNA−RNA heteroduplex. The whole length of 23S rRNA was analyzed with cDNAs proven to be effective at providing efficient sites of RNase-H cleavage. Positive results obtained are displayed in Figure 3.

RNase-H digestion of 23S RNA photolabeled with PHONT **1** revealed site-specific photoincorporation into three regions. The ~400 nt and ~600 nt fragments seen in lanes 3−5 demonstrate photoincorporation into two of these, nts 2501−2904 and 1887−2501, respectively. As digestion of 23S rRNA in the presence of cDNA 2639−23 failed to generate a labeled fragment of ~270 nt, (data not shown) the first labeled region can be further localized to between 2501 and 2631, which includes the target site. The second labeled region can be further localized to between nts 1887 and 1966, on the basis of the ~85 nt fragment seen in lanes 6−8 and the absence of a labeled fragment of ~350 nt on digestion of labeled 23S rRNA in the presence of cDNAs 1971−62 and 2310−01 (data not shown). The labeled fragment centered at ~63 nt in lanes 6−8 is due to an intrinsic cleavage site at nt 1915 (*22*) coupled with the RNase-H site induced by cDNA 1971−62. The third region falls between nts 861 and 1046, as demonstrated by the labeled fragment of ~200 nt in lanes 9−11. This site can be further localized to between nts 861 and 911 by the ~63 nt fragment seen in lanes 12−14 and the absence of a labeled fragment of ~150 nt on digestion of labeled 23S rRNA in the presence of cDNAs 916−07 and 1051−42 (data not shown).

In contrast with PHONT **1**, PHONT **2** photoincorporated site-specifically into only a single region of 23S rRNA, between nts 2305 and 2501, as shown by the labeled 200 nt fragment in lanes 15−17.

Identification of Labeled Nucleotides. Specific sites of photoincorporation within the labeled fragments were identified by reverse transcriptase primer extension on 23S rRNA extracted from 50S subunits photolabeled by PHONTs **1** or **2**. These experiments were carried out with excess PHONT over 50S subunit in order to maximize the stoichiometry of probe photoincorporation, thereby increasing the visibility of autoradiographic bands arising from primer extension stops or pauses (Figure 4). Sites of photoincorporation are the nucleotides immediately following stop or pause sites (−1 in the 23S rRNA sequence).

Five primers were employed to identify incorporation sites of PHONT **1**. Primer extension using cDNA 2639−23 identified C2601, U2586, and U2563 as major sites of

Table 1: Overall PHONT Photoincorporation[a]

sample	PHONT	standard[b]	prephotolysis	standard + complementary 2′-O-Me-oligo RNA[c]	standard + MM-2′-OMe-oligo RNA[d]
23S rRNA[e]	1	2.3 ± 0.4	0.17 ± 0.04	0.4 ± 0.1	1.5 ± 0.3
23S rRNA[e]	2	4.0 ± 0.6	0.17 ± 0.03	0.4 ± 0.1	2.1 ± 0.1
TP 50[f]	1	1.3 ± 0.2	nd[g]	0.9 ± 0.2	1.0 ± 0.1
TP 50[f]	2	0.8 ± 0.2	nd	0.8 ± 0.2	0.7 ± 0.1

[a] Numbers shown are pmol of the PHONT. [b] In the standard experiment, 300 pmol of 50S subunits and 20 pmol of PHONT were photolyzed. In the prephotolyzed control, PHONT was photolyzed prior to mixing with 50S subunits and there was no subsequent photolysis. [c] 3 nmol of 2′-O-methyloligoRNA-2612−04 or 2′-O-methyloligoRNA-2458−48 was added prior to photolysis. [d] 3 nmol of MM-2′-O-methyloligoRNA-2612−04 or MM-2′-O-methyloligoRNA-2458−48 was added prior to photolysis. [e] Estimated from radioactivity precipitated with 23S rRNA. [f] Estimated from radioactivity eluting with 50S proteins on RP-HPLC. [g] nd = not detectable.

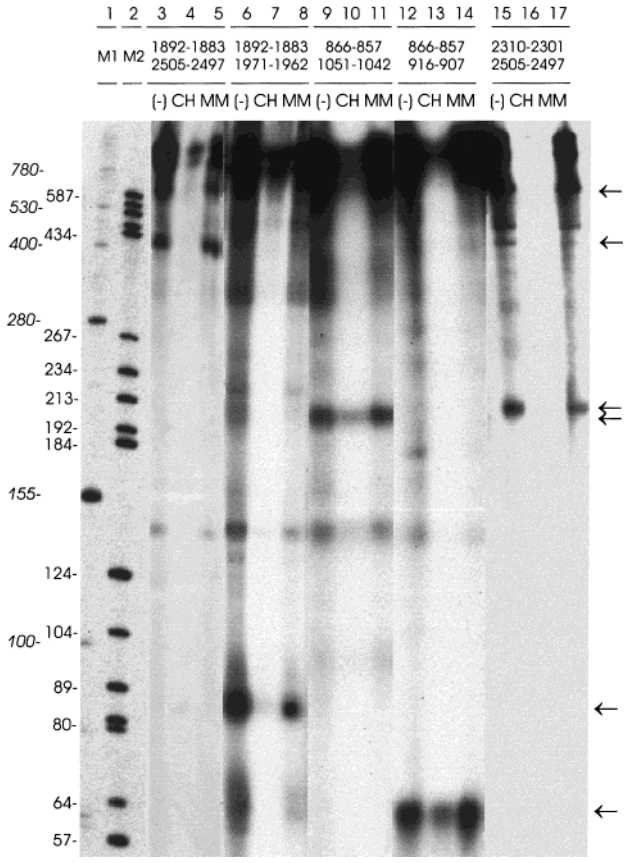

FIGURE 3: RNase-H digestion of PHONT-labeled RNA. Labeled RNA (8−10 pmol), isolated from 50S subunits photolyzed in the presence of PHONT **1** or **2**, was incubated with two equivalents of the indicated cDNA probe(s) and digested with 2 units of RNase-H in 10 μL of TND buffer containing 10 mM Mg^{2+}. The cleavage products were electrophoresed on a 5% polyacrylamide/0.25% bis-(acrylamide)/7 M urea gel made up in TBE buffer. Radioactive fragments were visualized by autoradiography. Photolabeling experiments were carried out either in the absence of competitor 2′-O-methyloligoRNA [lanes (−)], or in the presence of a 10-fold excess (over 50S subunit) of 2′-O-methyloligoRNA either complementary to 23S rRNA nucleotides 2604-12 or 2448-58 (lanes CH) or containing mismatches (lanes MM). Lane 1: RNA size markers. Lane 2: DNA size markers, with sizes (in nt) indicated to the left of the gel. RNA sizes are italicized. Lanes 3−14, 23S rRNA labeled with PHONT **1**. Lanes 3−5, with cDNAs 1892−83 and 2505−2497; lanes 6−8, with cDNAs 1892−83 and 1971−62; lanes 9−11, with cDNAs 866−57 and 1051−42; lanes 12−14, with cDNAs 866−57 and 916−07. Lanes 15−17, 23S rRNA labeled with PHONT **2**, digested with cDNAs 2505−2497 and 2310−01.

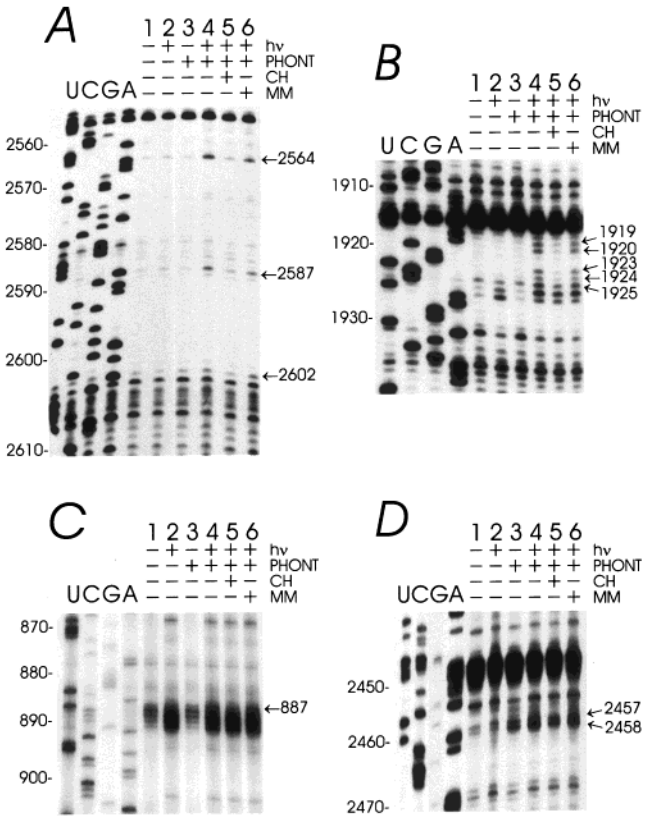

FIGURE 4: Reverse transcriptase analyses of PHONT-labeled 23S rRNA. Photoincorporation was performed using 50S subunits (150 pmol) and either PHONT **1** (375 pmol) or PHONT **2** (1500 pmol) in the absence or presence of a 3-fold excess (1125 pmol for **1**; 4500 pmol for **2**) of added complementary 2′-O-methyloligoRNA (CH) or of mismatched 2′-O-methyloligoRNA (MM), as indicated, in a reaction volume of 150 μL. Analyses *A* -*C* and *D* were performed on 23S rRNA labeled with PHONTs **1** and **2**, respectively. The cDNA primers used were: A, 2639-23; B, 1983-65; C, 1040-24; D, 2576-60. Lanes U, C, G, and A are sequencing products generated from control 23S rRNA in the presence of ddATP, ddGTP, ddCTP, and ddTTP, respectively. Indicated with arrows are nts at which pauses or stops induced by site-specific photoincorporation of PHONT **1** or **2** are observed.

photoincorporation (Figure 4A). Similar analyses with cDNA primers 1983−1965 and 1040−1024 permitted identification of nts A1918, A1919, G1922, U1923, C1924 (Figure 4B), and A886 (Figure 4C), respectively, as photoincorporation sites. Each of these sites is labeled site-specifically, as demonstrated by the much larger decreases in stop intensity seen in the presence of competing complementary 2′-O-methyloligoRNA vs those seen in the presence of mismatched 2′-O-methyloligoRNA. No further incorporation sites were identified using either cDNA 2042-26 or 918-01 as primers.

For PHONT **2**, primer extension using cDNA 2576-60 gave evidence for site-specific photoincorporation into ψ2457 and C2456 within the target site (Figure 4D). No other

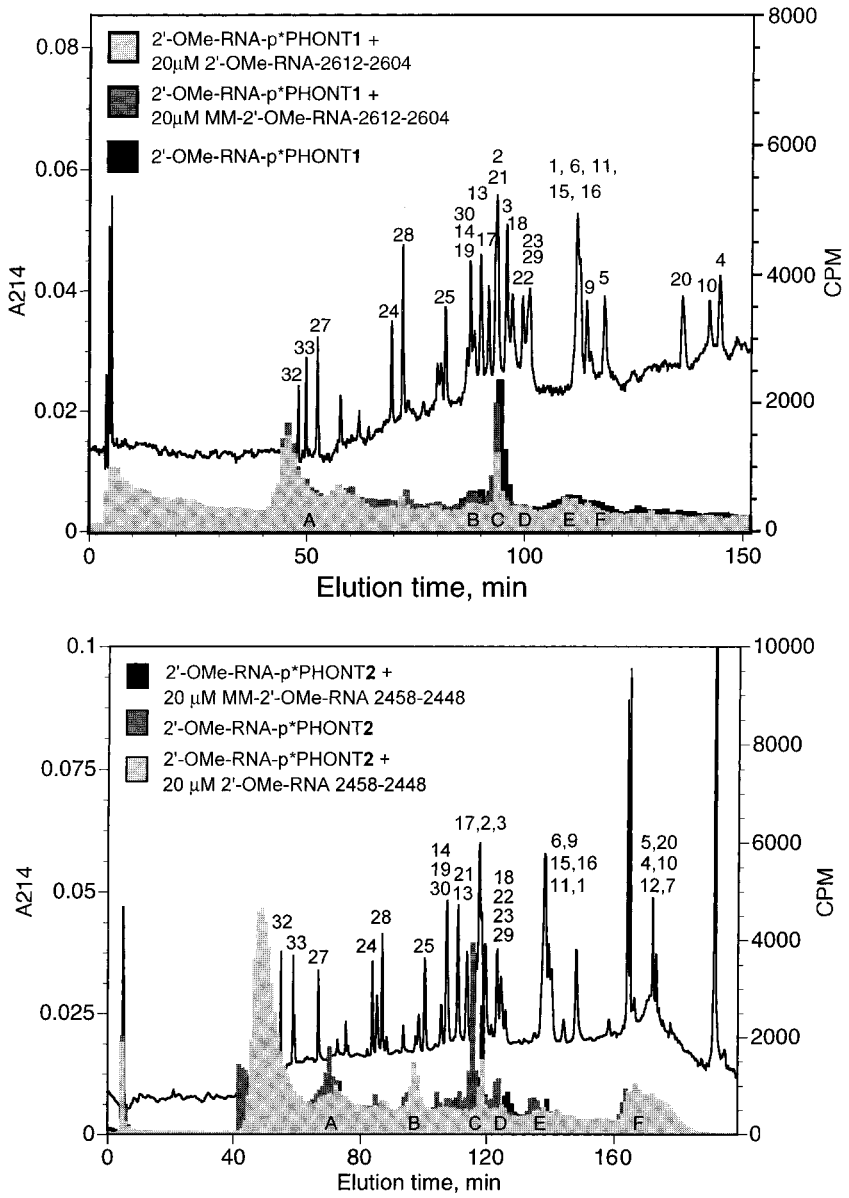

FIGURE 5: RP-HPLC analyses of PHONT-labeled TP50. TP50 was extracted from 50S subunits labeled with PHONT in the absence or presence of either competitive complementary 2′-O-methyloligoRNA or MM-2′-O-methyloligoRNA, under the conditions described in Table 1. For each analysis, proteins were extracted from photolyzed subunits with 67% acetic acid, precipitated with 5 volumes of acetone, redissolved in 200 μL of 0.1% TFA, applied to a SynChropack RP-P reverse-phase C18 column, and eluted at a flow rate of 0.7 mL/min with a 120-min 15−45% convex acetonitrile gradient containing 0.1% TFA. (A) Labeled with PHONT **1**. (B) Labeled with PHONT **2**. For clarity, radioactivity for PHONT **2** alone is offset by 3 min relative to PHONT **2** in the presence of either complementary 2′-O-methyloligoRNA or MM-2′-O-methyloligoRNA.

incorporation sites were identified using either cDNA 2493-77 or 2443-27 as primers.

Identification of Specifically Labeled 50S Proteins. Site-specifically labeled proteins were identified by combining RP-HPLC and SDS-PAGE analyses. We have previously shown that ribosomal proteins covalently labeled with oligonucleotides elute on RP-HPLC with or close to unmodified proteins and migrate in SDS-PAGE with apparent masses approximately equal to the sum of the masses of the labeled protein and of the attached oligonucleotide (*4*−*7*, *18*), which are 3.4 and 4.0 kDa for PHONTs **1** and **2**, respectively.

RP-HPLC analyses of TP50 extracted from 50S subunits labeled with PHONTs **1** and **2** are shown in Figure 5. In both cases, the major radioactive peak eluted with or close to proteins L2 and L3 and in both cases photoincorporation into this peak was site-specific. For PHONT **1**, SDS-PAGE analysis of labeled TP50 revealed the presence of at least seven labeled bands (Figure 6, lanes 1−4, I−VII) of which only one, the uppermost band I, is labeled site-specifically. SDS-PAGE analysis was also performed on RP-HPLC fractions corresponding to peaks A−F in Figure 5A. Peak C, eluting amidst proteins L2, L3, L17, L18, and L21, shows site-specific labeling of band I (Figure 6, lanes 5−7). No other peaks show site-specific labeling (data not shown), consistent with the results for TP50. Band I can be identified as corresponding to labeled L2, on the basis of its elution position and its apparent mass of 38.9 kDa, as determined from a plot of log mass vs migration. Unmodified L2 [actual mass 29.7 kDa (*23*)] migrates with an apparent mass of 34.9 kDa.

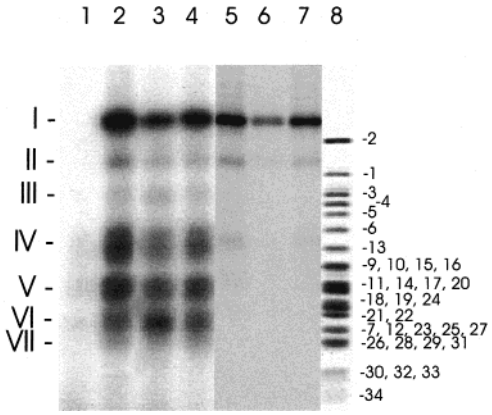

FIGURE 6: Autoradiogram of SDS-PAGE analyses of PHONT 1-labeled TP50 and RP-HPLC peak C (see Figure 5A). Lanes 1−4 are for TP50, lanes 5−7 are for peak C. Lane 1: 50S subunits were incubated with prephotolyzed PHONT **1** with no further photolysis. Lanes 2 and 5: subunits photolyzed with PHONT **1**. Lanes 3, 4, 6, 7: subunits photolyzed with PHONT **1** in the presence of 10-fold excess (over 50S subunits) of either 2′-O-methyloligoRNA-2612-04 (lanes 3 and 6) or MM-2′-O-methyloligoRNA-2612-04 (lanes 4 and 7). Lane 8: TP50 stained with Coomassie Blue.

Table 2: Summary of Site-specific Crosslinks from PHONTs 1 and 2

crosslink #	PHONT **1** (2604) to:	crosslink #	PHONT **2** (2448) to:
1	A886	7a	C2456
2a	A1918	7b	Ψ2457
2b	A1919	8	L2
2c	G1922	9	L3
2d	U1923	10	(L17/L18/L21)[a]
2e	C1924	11	(L9/L15/L16)[a]
3	U2563		
4	U2586		
5	C2601		
6	L2		

[a] One or more of the proteins within parentheses are cross-linked. See text.

SDS-PAGE analysis of TP50 labeled with **2** showed three major bands (I′, II′, and III′) to be labeled site-specifically (Figure 7, lanes 2−5). Three major specifically labeled bands, corresponding to I′, II′, and the lower half of III′ (denoted IIIb′) are also seen on SDS-PAGE analysis of RP-HPLC fractions corresponding to the combined peaks C/D (lanes 6−8). A fourth major specifically labeled band, corresponding to the upper half of III′ (denoted IIIa′) is seen on SDS-PAGE analysis of RP-HPLC fraction E (lanes 9−11). Fractions A, B, and F did not contain major specifically labeled bands (data not shown). Bands I′ and II′ are readily identified by elution position and apparent mass, as above, as labeled L2 and L3, respectively. However, we have not as yet definitively identified labeled proteins in bands IIIa′ and IIIb′. The plausible candidates for IIIa′ are labeled L9, L15, or L16 and for IIIb′ labeled L17, L18, or L21.

Effects of 2′-O-MethyloligoRNAs on Chemical Footprinting of 23S rRNA. To assess whether PHONT binding to the 50S subunit causes structural distortions outside of the expected local distortion at its binding site, we examined the effects of noncovalent binding of the 2′-O-methyloligoRNAs 2612-04 and 2458-48, and of PHONT **1**, on chemical footprinting (dimethyl sulfate and kethoxal) patterns in regions of 23S rRNA (nts 750−1130, 1780−2650) that either include the cross-linking sites identified above (Table 2) or that have been implicated either directly or indirectly in peptidyl transferase activity (*9*, *10*, *12*, *24*−*29*). For purposes of comparison, we also examined the effects of noncovalent binding of 2′-O-methyloligoRNA 2258-53/52-(S)-48 (see Materials), which we have shown to bind to its target site (*8*).

Outside of stops (or pauses) at or immediately adjacent to their target sites, none of the four 2′-O-methyloligoRNAs show effects on chemical footprinting patterns from nts 2216−2651 (Figure 8). Similarly, no changes were seen for nts 750−970 (data not shown), although PHONT **1,** and its parent 2′-O-methyloligoRNA 2612-04, both induce stops at nts A1008 (Figure 9A) and U1926 (Figure 9D) even in the absence of chemical modification. Moreover, footprinting changes are induced in regions 991−1058 (Figure 9A), 2006−2020 (Figure 9B), and 2170−2215 (Figure 9C), as well as at nts A1928 and G1929 (Figure 9D) and C2072, C2089, and C2091 (Figure 9C), by the binding of each of the four 2′-O-methyloligoRNAs.

We demonstrated that these latter changes are not specific for oligonucleotides bound to the peptidyl transferase center by examining the effect on footprinting in regions 991−1058 and 2170−2215 of adding oligonucleotides that were: (a)

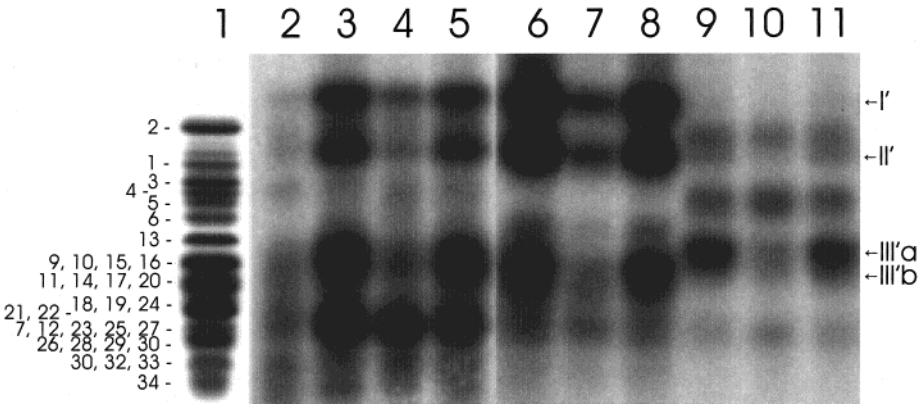

FIGURE 7: Autoradiogram of SDS-PAGE analyses of PHONT 2-labeled TP50 and RP-HPLC peaks (see Figure 5B). Lane 1: TP50 stained with Coomassie Blue. Lanes 2−5 are for TP50, lanes 6−8 are for peak C/D, lanes 9−11 are for peak E. Lane 2: 50S subunits were incubated with prephotolyzed PHONT **2** with no further photolysis. Lanes 3, 6, and 9: subunits photolyzed with PHONT **2**. Lanes 4, 5, 7, 8, 10, and 11: subunits photolyzed with PHONT **2** in the presence of 10-fold excess (over 50S subunits) of either 2′-O-methyloligoRNA-2458-48 (lanes 4, 7, and 10) or MM-2′-O-methyloligoRNA-2458-48 (lanes 5, 8, and 11).

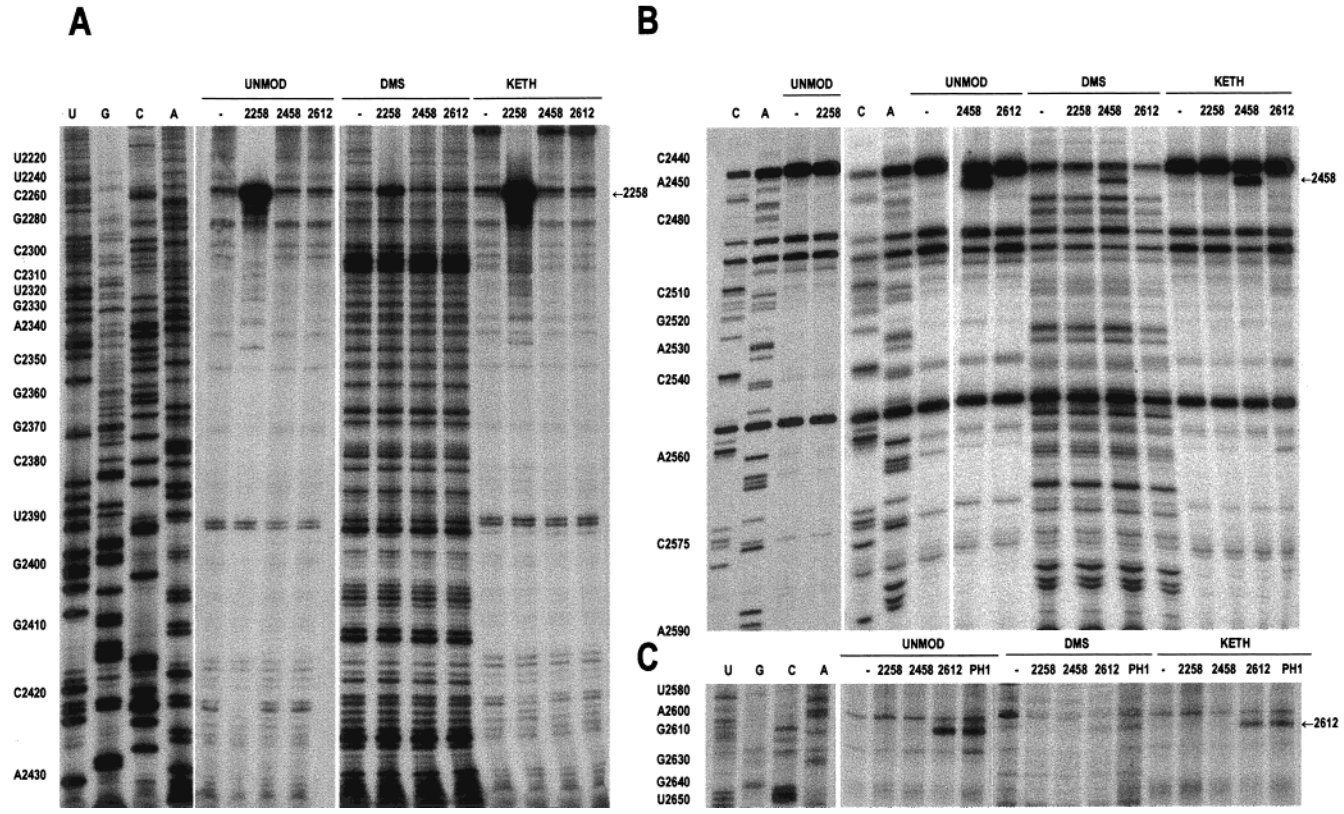

FIGURE 8: Primer extension analysis of the effects of 2′-O-methyloligoRNA binding on chemical footprinting of the peptidyl transferase region within 50S subunits. In both panels, lanes U, G, C, and A are sequencing products generated from control 23S rRNA in the presence of ddATP, ddCTP, ddGTP, and ddTTP, respectively. Lanes (−) are for incubations of 50S subunits conducted in the absence of 2′-O-methyloligoRNA; lanes 2258, 2458, 2612, and PH1 are for incubations conducted in the presence of 2′-O-methyloligoRNAs 2258-53/52-(S)-48, 2458-48, 2612-04, or PHONT **1**, respectively. Lanes UNMOD, DMS, and KETH are for incubations in the absence of chemical modification, in the presence of dimethyl sulfate, or in the presence of kethoxal, respectively. The oligo DNA primers used for extension were: Panel A: 2457-42. Panel B: 2639-23. Panel C: 2787−71.

complementary to a 23S rRNA sequence not thought to be part of the peptidyl transferase center (2′-O-methyloligoRNA-782-72); (b) complementary to 16S rRNA sequences (cDNA-1531-22 and 2′-O-methyloligoRNA-1405-02/1(S)-1397); (c) designed to have four mismatches with 23S rRNA sequence 2248−58 (MM-2′-O-methyloligoRNA-2258-48). In each case, chemical footprinting patterns essentially identical to those presented in Figure 9A,C were observed (data not shown). Extensive dialysis of these oligonucleotides [using YM-3 (Amicon) membranes having a 3000 molecular weight cutoff] prior to their use in the footprinting experiment did not affect these results, ruling out the possibility of an artifact due a common impurity in synthetic oligonucleotides. These changes are further considered below (see Discussion).

DISCUSSION

Confidence that the 11 photocrosslinks summarized in Table 2 define ribosomal components that fall within 25 Å of either U2604 or A2448 comes from three principal lines of evidence. First, the strong photoincorporation of each PHONT at or near its target site (cross-links no. 5 and 7) shows that at least part of the binding seen in Figure 2 takes place at the target site. Second, and more compellingly, the yields of photocrosslinked RNase-H fragments (Figure 3), nucleotides (Figure 4), and proteins (Figures 5−7) are decreased much more strongly in the presence of competing complementary 2′-O-methyloligoRNA than in the presence of mismatched 2′-O-methyloligoRNA. Finally, scanning the 23S rRNA sequence using AMPLIFY (www.wisc.edu/genestest/CATG/amplify (accessed most recently Nov. 1999)) showed that, outside of the target regions, the best matches to either PHONT **1** or **2** contained at least three mismatches, making photoincorporation from such sites very unlikely.

Since we seek to generate photocrosslinks that will be useful in constructing and evaluating models of the peptidyl transferase center within the 50S subunit, it is also important to assess to what extent PHONT binding to the 50S subunit causes structural distortions outside of the expected local distortion at its binding site. In this respect, the result that noncovalent binding of the 2′-O-methyloligoRNAs 2612-04 and 2458-48, and of PHONT **1** cause no significant chemical footprinting changes between nts 2215−2650 at other than the target sites is particularly important. This region includes all of those portions of 23S rRNA most directly associated with peptidyl transferase activity, so that the absence of chemical footprinting changes strongly suggests that binding of these 2′-O-methyloligoRNAs induces no major distortion of the peptidyl transferase center. Support for this suggestion comes from earlier work of Hill and co-workers (*30*), showing no effect of cDNA 2613-06 binding to the 70S ribosome on $tRNA^{Phe}$ binding or of cDNA 2614-07 binding on in vitro translation. Similarly, cross-link #1 between PHONT **1** and A886 is unlikely to be attributable to a distortion in 50S structure, since no chemical footprinting changes are seen between nts 750 and 970 on 2′-O-methyloligoRNA 2612-04 or PHONT **1** binding.

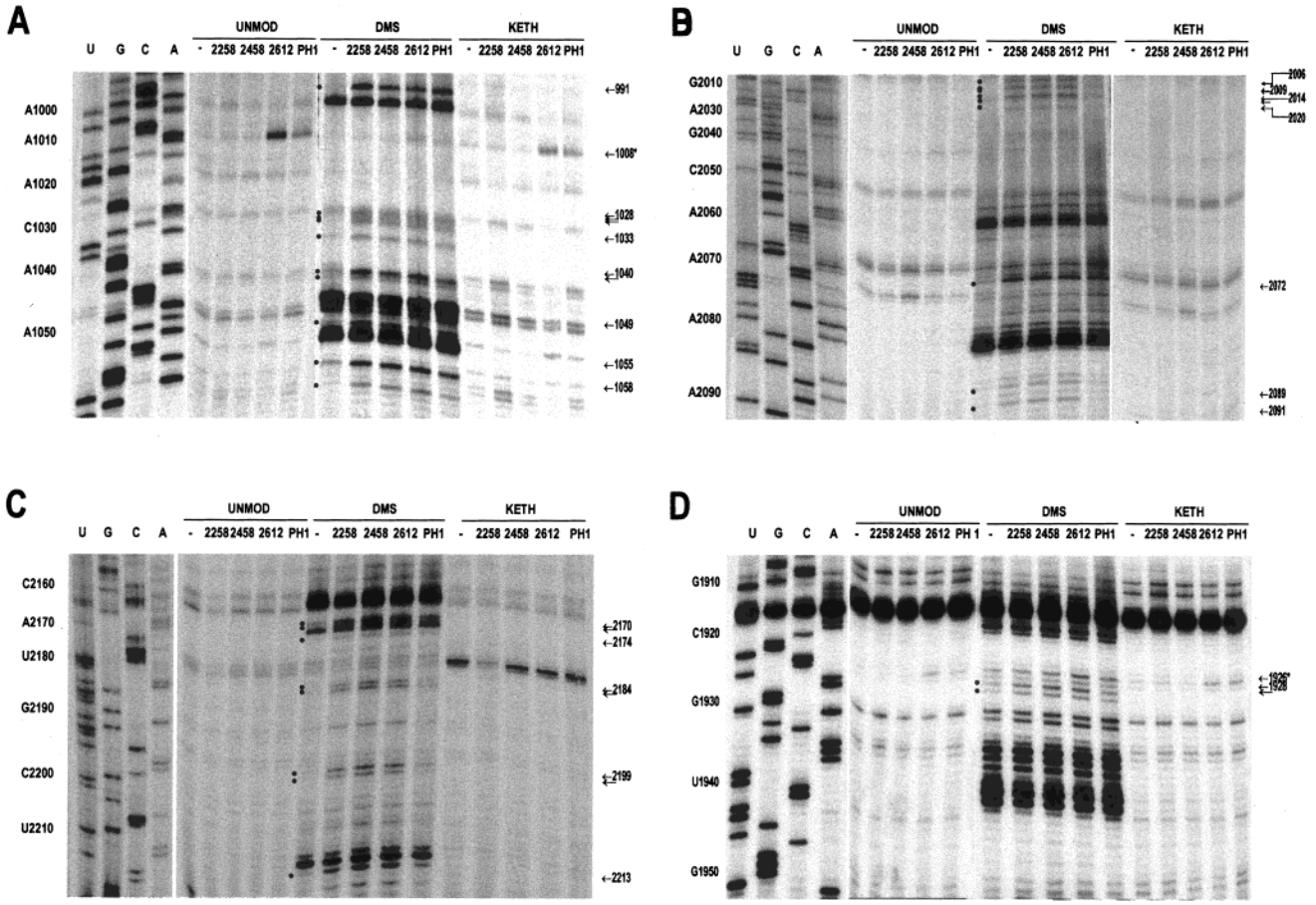

FIGURE 9: Primer extension analysis of the effects of 2′-O-methyloligoRNA binding on chemical footprinting outside of the target regions for PHONTs **1** and **2**. Lane headings as in Figure 8. The oligo DNA primers used for extension were: Panel A: 1115−1099. Panel B: 2125−09. Panel C: 2250−34. Panel D: 1983−65. Double and triple arrows indicate stops at consecutive nts. Bullets in the middle of the panels are aligned with arrows on the right. The stops marked with an asterisk (1008 − panel A and 1926 − panel D) are seen in both the absence and presence of chemical modification. The apparent reduction in intensity of the stops at 2180 and 2181 in the KETH/2258 lane (panel C) is an artifact. No such reduction was seen in other extension experiments.

On the other hand, PHONT **1** and 2′-O-methyloligoRNA 2612-04 do induce a weakly enhanced stop at U1926 (Figures 4B, 9D-unmodified lanes), not induced by the 2′-O-methyloligoRNAs 2458-48 and 2258-53/52(S)-48, that is immediately adjacent to the stops grouped together as cross-link #2. These results suggest a physical proximity between nts U2604−C2612 and A1918−C1925 that is manifested both by an induced change in RT extension and by the formation of cross-link no. 2.

Also of interest are the chemical footprinting changes induced on addition not only of the four 2′-O-methyloligoRNAs that bind to the peptidyl transferase center (Figure 9), but also of the other four oligonucleotides (9−11 nts long) tested. These results raise two interesting questions, the answers to which remain conjectural. Why do the footprinting changes occur? Do the identities of the 23S rRNA nucleotides showing enhanced chemical reactivity on oligonucleotide addition tell us something about 50S structure?

The generality of the nonsequence specific footprinting changes suggests a procedural artifact of as yet unknown origin. One possibility is that such changes arise from even weak oligonucleotide binding to 50S subunits. Such binding is evident in the biphasic nature of the binding curves in Figure 2. In our experience (*4*−*8*, *18*), such curves are characteristic of oligonucleotide binding to ribosomal subunits, and are attributable, at least in part, to oligonucleotide binding to secondary sites. The higher than 1:1 stoichiometry for 2′-O-methyloligoRNA- p*2612-04 binding to 50S subunits at very high oligonucleotide/50S ratios added to the reaction mixture (Figure 2) provides direct evidence for secondary sites. Such sites could arise from binding to 23S rRNA regions in which complementarity is less than perfect [cDNA-1531-22 has six matches of seven nts with 23S rRNA, 2′-O-methyloligoRNA-1405-02/1(S)-1397 has one match of eight nts and one of seven nts, MM-2′-O-methyloligoRNA-2258-48 has one match of nine nts and six matches of eight nts], or to ribosomal protein (see the nonspecific protein labeling in Figures 5−7), or to a mix of both.

Irrespective of the underlying reasons for nonsequence specific footprinting changes, it is an intriguing speculation that the nucleotides showing such changes fall in flexible "hinge" regions that open up and become more available for chemical modification on oligonucleotide addition. One of the regions showing such changes, nts 2169−2212, contains several sites that cross-link to L1 (*31*), and the L1 protein region has been shown by cryo-electronmicroscopy studies to be one of the most flexible regions in the 50S subunit (*32*). A second region, which includes nts 1039, 1040, 1048, 1054, and 1057, overlaps with a 58 nt 23S rRNA domain (nts 1051−1108), the structure of which is stabilized by the binding of protein L11 to two stem-loop regions

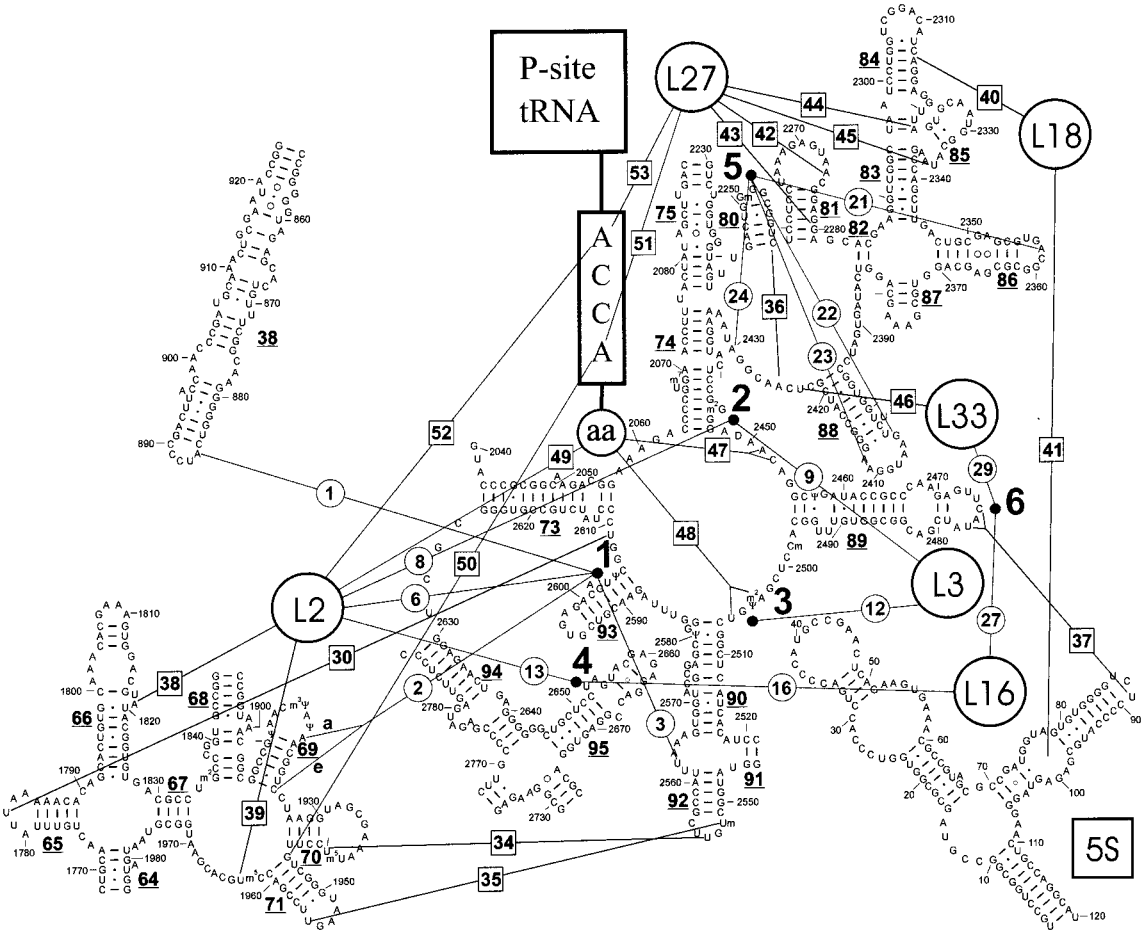

FIGURE 10: Summary of cross-linking results useful for construction of a peptidyl transferase model. Cross-links shown are numbered according to Tables 2−4. Large bold numbers refer to target sites for the PHONTs described in Tables 2 and 3, giving rise to circled cross-links. Boxed cross-links are formed using other approaches (Table 4). Helices (underlined) are numbered as in ref *26*.

contained within it (*33*, *34*). Conformational flexibility of the 1067 and 1095 loops is suggested by biochemical evidence that they are interaction sites for both thiostrepton and EF-G (*35*, *36*).

Comparison of Cross-linking Results with Related Results of Others. Six of the cross-links (no. 1−3, 6, 8, and 9) in Table 2 are significant for identifying ribosomal components neighboring the central loop of domain V [we exclude cross-links no. 10 and 11 because of their incomplete identification; also, cross-link 4 only confirms the standard model (*38*) for the secondary structure of 23S rRNA (Figure 10), in which helix 93 brings U2586 close to U2604]. Of these, cross-links no. 1, 2, 6, and 8 are supported by studies employing tRNA or tRNA analogues and photo- (ϕXL) or electrophilic cross-linking (EXL), chemical footprinting (FP), and induced chemical cleavage (CC). Here, the reasoning is that interaction with different 50S components from a common reference location, in this instance the 3′-end of P-site bound tRNA, from nucleotide A_{73} through the attached amino acid, provides evidence for the proximity of the components in question. These tRNA studies yield results linking central loop positions A2451 [ϕXL, FP (*11*, *27*)], C2452, A2503, and U2506 [ϕXL (*11*)] and A2602 [FP, CC (*27*)] with 23S rRNA positions A1916, A1918, U1926 [FP (*27*)], and with protein L2 [ϕXL, EXL (*39*−*41*)]. The low peptidyl transferase activity resulting from U1926C mutation (*42*) is also consistent with cross-link no. 2. Similarly, a photolabile derivative at position 47 of A-site bound Phe-tRNA links C2452 with as yet unidentified nucleotides falling within the 23S rRNA sequences 865−910 and 1892−1945 [XL (*43*)] consistent with cross-links no. 1 and 2. A more precise overlap with cross-link no. 1 comes from a study employing RNA helices of varying length attached to a P-site bound anticodon loop (so-called "ASLs"). These are derivatized with an Fe−EDTA group and induce chemical cleavages at varying distances from the anticodon loop binding site. Using the same size ASLs (4−12 bps), cleavages are induced at or close to A2602 in the central loop and at or close to G880 and C890 [CC (*44*)].

Supporting evidence for cross-link no. 3 is provided by both cross-linking and mutation studies showing the importance of helix 92 (Figure 10) for PT activity (*45*, *46*). Finally, with respect to cross-link no. 9, our current results reaffirm the proximity of L3 to the central loop that was first indicated by the finding that L3 was labeled by PHONT **3** targeted toward nts 2497−2505 (Table 3). Placement of L2 and L3 at or near the central loop is also consistent with partial reconstitution studies demonstrating that of all ribosomal proteins, only L2 and L3 could be essential for PT activity (*29*, *47*). We and others have provided evidence for a direct role of L2 in such activity (*25*, *48*).

Toward a Three-dimensional Model of the Peptidyl Transferase Center (*PTC*). The PTC has been a popular target for topological studies because of the central place of peptidyl

Table 3: Site-specific Crosslinks from Other Oligonucleotide PHONTs at or near the Peptidyl Transferase Center[a]

crosslink no.	PHONT **3** (2505)[b] to:
12	L3
	PHONT **4** (2653)[c] to:
13	L2
14	L1
15	L15
16	L16
17	(L5)
18	(L9)
19	(L17)
20	(L24)
	PHONT **5** (2252)[d] to:
21a	G2357
21b	A2358
22a	U2404
22b	G2405
22c	A2406
23	A2411
24	A2430
	PHONT **6** (2475)[e] to:
25	L1
26	L13
27	L16
28	L32
29	L33

[a] Excluded are cross-links at the target site or very close to it in the standard model for 23S rRNA 2° structure (38). Proteins in parentheses are labeled to minor extents. [b] Ref 4. [c] Ref 6. [d] Ref 8. [e] Ref 5.

Table 4: Other Intra-50S Cross-links at or near the Peptidyl Transferase Center

crosslink no[a]	RNA−RNA[b]
30	1782-2608/9
31	1911/1921-1964
32	1933-1966
33	1941/2-1964/5
34	1940-2554
35	1955-2552/3
36	2257/65-2425/7
37	2475, 2477-89(5 S)
	protein−RNA[b]
38	L2-1818/23
39	L2-1963
40	L18-2307/20
41	L18-1/120 (5 S)
42	L27-2272/6
43	L27-2276/83
44	L27-2320/23
45	L27-2332/37
46	L33-2422/24
	3′-end of P-site bound tRNA: $A_{73}CCA_{76}$-aa[c]
47	aa-2451/52
48	aa-2503/06
49	aa-L2
50	A_{76}−G1945
51	A_{76}−L27
52	A_{73}−L2
53	A_{73}−L27

[a] References to specific cross-links: #s 30, 33, 34, 35 ref *37*; #s 31, 32, ref *57*; # 36, ref *58*; # 37, ref *24*; #s 38, 40−44, ref *31*; # 39, ref *54*; #s 45, 46, ref *59*; #s 47, 48, ref *11*; # 49, ref *41*; # 50, ref *60*; #s 51−53, ref *39*. [b] Nucleotide #s are for 23S rRNA unless otherwise indicated. [c] Amino acid attached at the 3′-end of tRNA.

transferase in ribosomal function. In turn, the abundance of results obtained from such studies makes the PTC a particularly attractive object for three-dimensional model construction, as has been done for the 30S subunit (*49*, *50*). Comparison of such a model with electron density maps emerging from crystallographic (*1*, *3*) and electron microscopy (*51*) studies should allow for clear placement of the PTC region within the ribosome. Although deciding which 50S components to include in modeling the PTC region is necessarily somewhat arbitrary, examination of the pertinent literature (much of which is reviewed or tabulated in refs *9*, *10*, *12*, *24*−*29*) leads to the following choices. With respect to rRNA, the central loop of domain V; the stem-loops corresponding to helices 38, 65−67, 69−71, 74, 80, 84, 86−90, 92−95; and 5S rRNA (Figure 10). With respect to proteins, L2, L3, L15, L16, L18, L23, L27, and L33.

Cross-linking results provide an important set of constraints for model construction. The results of the current work (Table 2) provide a new set of six such constraints for PTC modeling. Earlier cross-linking results (Tables 3 and 4) provide further constraints. These include: (a) 11 cross-links identifying components within 17−26 Å of nts G2505, U2653, G2252, and C2475, obtained using PHONTs, in work similar in kind to that presented here; (b) 17 RNA−RNA and RNA−protein cross-links; (c) seven cross-links from the 3′-end of tRNA to both 23S rRNA and ribosomal proteins. There are, in addition, some 13 cross-links among the eight proteins listed above (*52*, *53*), but these are currently less useful for model building.

The most useful constraints for modeling the PTC are summarized in Figure 10. Although modeling efforts are currently underway, we expect that construction of a reliable model will require additional information. Such information should be forthcoming in part via the use of additional photolabile oligonucleotide probes, especially those targeted toward less well-determined areas of the PTC. In addition, determination of sites of protein cross-linking at the amino acid level, as described by Wittmann-Liebold and her colleagues (*54*), will allow better protein placement within models. The importance of such information would be enhanced by the eventual availability of known structures of isolated ribosomal proteins, since, as has been demonstrated recently for protein L1, such structures can be used to fit specific electron density in high-resolution X-ray crystallographic and electron microscopy structures (*1*−*3*, *41*). Thus far, only a partial structure of one of the structures of the eight 50S proteins listed above, L2, has been reported (*55*). However, this is an active field of research (*56*) and it is reasonable to assume that at least some of these structures will soon be available.

ACKNOWLEDGMENT

We gratefully acknowledge the excellent technical assistance of Ms. Nora Zuño in several aspects of this work.

REFERENCES

1. Cate, J. H., Yusupov, M. M., Yusupova, G. Z., Earnest, T. N., and Noller, H. F. (1999) *Science* 285, 2095−2104.
2. Clemons, W. M. Jr, May, J. L., Wimberly, B. T., McCutcheon, J. P., Capel, M. S., and Ramakrishnan, V. (1999) *Nature* 400, 833−840.
3. Ban, N., Nissen, P., Hansen, J., Capel, M., Moore, P. B., and Steitz, T. A. (1999) *Nature* 400, 841−847.

4. Muralikrishna, P., and Cooperman, B. S. (1991) *Biochemistry* 30, 5421−5428.
5. Muralikrishna, P., and Cooperman, B. S. (1994) *Biochemistry* 33, 1392−1398.
6. Muralikrishna, P., Alexander, R. W., and Cooperman, B. S. (1997) *Nucleic Acids Res*. 25, 4562−4569.
7. Alexander, R. W., and Cooperman, B. S. (1998) *Biochemistry* 37, 1714−1721.
8. Bukhtiyarov, Y., Druzina, Z., and Cooperman, B. S. (1999) *Nucleic Acids Res*. *27*, 4376−4384.
9. Cooperman, B. S., Weitzmann, C. J., and Fernández, C. L. (1990) In *The Ribosome*: *Structure, Function, and Evolution* (Hill, W. E., Dahlberg, A., Garrett, R. A., Moore, P. B., Schlessinger, D., and Warner, J. R., Eds.) pp 491−501, American Society for Microbiology, Washington, D. C.
10. Garrett, R. A., and Rodriguez-Fonseca, C. (1996) In *Ribosomal RNA*: *Structure, Evolution, Processing, and Function* (Zimmermann, R. A., and Dahlberg, A., Eds.). pp 327−355, CRC Press, Boca Raton, FL.
11. Barta, A., and Halama, I. (1996) In *Ribosomal RNA and Group I Introns* (Green, R., and Schroeder, R., Eds.) pp 35−54, R. G. Landes Company, Austin, TX.
12. Green, R., and Noller, H. F. (1997) *Annu. Rev. Biochem*. 66, 679−716.
13. Porse, B. T., and Garrett, R. A. (1995) *J. Mol. Biol*., 249, 1−10.
14. Cundliffe, E. (1990) In *The Ribosome*: *Structure, Function, and Evolution* (Hill, W. E., Dahlberg, A., Garrett, R. A., Moore, P. B., Schlessinger, D., and Warner, J. R., Eds.) pp 479−490, American Society for Microbiology, Washington, D. C.
15. Hall, C. C., Johnson, D., and Cooperman, B. S. (1988) *Biochemistry* 27, 3983−3990.
16. Moazed, D., and Noller, H. F. (1987) *Biochimie* 69, 879−884.
17. Rodriguez-Fonseca, C., Amils, R., and Garrett, R. A. (1995) *J. Mol. Biol*., 247, 224−235.
18. Alexander, R. W., Muralikrishna, P., and Cooperman, B. S. (1994) *Biochemistry* 33, 12109−12118.
19. Moazed, D., Stern, S., and Noller, H. F. (1986) *J. Mol. Biol*. 187, 399−416.
20. Inoue, H., Hayase, Y., Imura, A., Iwai, S., Miura, K., and Ohtsuka, E. (1987) *Nucleic Acids Res*. 15, 6131−6148.
21. Inoue, H., Hayase, Y., Iwai, S., and Ohtsuka, E. (1988) *Nucleic Acids Res*.*Symp. Ser*. 19, 135−138.
22. Branlant, C., Krol, A., Machatt, M. A., Pouyet, J, Ebel, J.-P., Edwards, K., and Kossel, H. (1981) *Nucleic Acids Res*. 9, 4303−4324.
23. Giri, L., Hill, W. E., Wittmann, H. G., and Wittmann-Liebold, B. (1984) *Adv. Prot. Chem*. 36, 1−78.
24. Dontsova, O., Tishkov, V., Dokudovskaya, S., Bogdanov, A., Döring, T.,Rinke-Appel, J., Thamm, S., Greuer, B., and Brimacombe, R. (1994) *Proc. Natl. Acad. Sci. U.S.A*. 91, 4125−4129.
25. Cooperman, B. S., Wooten, T., Romero, D. P., and Traut, R. R. (1995) *Biochem. Cell Biol*. 73, 1087−1094.
26. Brimacombe, R. (1995) *Eur. J. Biochem*. 230, 365−383.
27. Noller, H. F., Green, R., Heilek, G., Hoffarth, V., Hüttenhofer, A., Joseph, S., Lee, I., Lieberman, K., Mankin, A., Merryman, C., Powers, T., Puglisi, E. V., Samaha, R. R., and Weiser, B. (1995) *Biochem. Cell Biol*. 73, 997−1009.
28. Baranov, P. V., Kubarenko, A. V., Gurvich, O. L., Shamolina T. A., Brimacombe R. (1999) *Nucleic Acids Res*. 27, 184−5.
29. Khaitovich, P., Mankin, A. S., Green, R., Lancaster, L., and Noller, H. F. (1999)*Proc. Natl. Acad. Sci. U.S.A*. 96, 85−90.
30. Hill, W. E., Weller, J., Gluick, T., Merryman, C., Marconi, R. T., Tassanakajohn, A., and Tapprich, W. E. (1990) In *The Ribosome*: *Structure, Function, and Evolution* (Hill, W. E., Dahlberg, A., Garrett, R. A., Moore, P. B., Schlessinger, D., and Warner, J. R., Eds.) pp 253−261, American Society for Microbiology, Washington, D. C.
31. Osswald, M., Greuer, B., and Brimacombe, R.(1990) *Nucleic Acids Res*. 18, 6755−60.
32. Agrawal, R. K., Lata, R. K., Frank, J. (1999) *Int. J. Biochem. Cell. Biol*. 31, 243−254.
33. Conn, G. L., Draper, D. E., Lattman. E. E., and Gittis, A. G. (1999) *Science* 284, 1171−1174.
34. Wimberly, B. T., Guymon, R., McCutcheon, J. P., White, S. W., and Ramakrishnan, V. (1999) *Cell* 97, 491−502.
35. Thompson J., Cundliffe, E., and Dahlberg, A E. (1988) *J. Mol. Biol*. 203, 457−465.
36. Munishkin, A., and Wool, I. G. (1997) *Proc. Natl. Acad. Sci. U.S.A*. 94, 12280−12284.
37. Mitchell, P., Osswald, M., Schueler, D., and Brimacombe, R. (1990) *Nucleic Acids Res*. 18, 4325−33.
38. Gutell, R. R., Larsen, N., and Woese, C. R. (1994). *Microbiol. Rev*. 58, 10−26.
39. Wower, J., Rosen, K. V., Hixson, S. S., and Zimmermann, R. A. (1994) *Biochimie* 76, 1235−1246.
40. Graifer, D. M., Babkina, G. T., Matasova, N. B., Vladimirov, S. N., Karpova, G. G., and Vlassov, V. V. (1989) *Biochim. Biophys. Acta* 1008, 146−156.
41. Johnson, A. E., and Cantor, C. R. (1980) *J. Mol. Biol*. 138, 273−297.
42. Porse, B. T., Rodriguez-Fonseca, C., Leviev, I., and Garrett, R. A. (1995) *Biochem. Cell Biol*. 73, 877−885.
43. Osswald, M., Döring, T., and Brimacombe, R. (1995) *Nucleic Acids Res*. 23, 4635−4641.
44. Joseph, S., Weiser, B., and Noller, H. F. (1997) *Science* 278, 1093−1098.
45. Green, R., Samaha, R. R., and Noller, H. F. (1997) *J. Mol. Biol*. 266, 40−50.
46. Green, R., Switzer, C., and Noller, H. F. (1998) *Science* 280, 286−289.
47. Tate, W. P., Sumpter, V. G., Trotman, C. N. A., Herold, M., and Nierhaus, K. H. (1987) *Eur. J. Biochem*. 165, 403−408.
48. Uhlein, M., Weglöhner, W., Urlaub, H., and Wittmann-Liebold, B. (1998) *Biochem. J*. 331, 423−430.
49. Malhotra, A., and Harvey, S. C. (1994) *J. Mol. Biol*. 240, 308−340.
50. Wang, R. Alexander, R. W., van Loock, M., Vladimirov, S., Bukhtiyarov, Y., Harvey, S. C., and Cooperman, B. S. *J. Mol. Biol*. 286, 521−540.
51. Frank, J. (1998) *J. Struct. Biol*. 124, 142−50.
52. Traut, R. R., Tewari, D. S., Sommer, A., Gavino, G. R., Olson, H. M. Glitz, D. G. (1986) In *Structure, Function, and Genetics of Ribosomes*, (Hardesty, B., and Kramer, G., Eds.) pp 286−308, Springer-Verlag New York.
53. Walleczek, J., Martin, T., Redl, B., Stöffler-Meilicke, M., and Stöffler, G. (1989) *Biochemistry* 28, 4099−4105.
54. Thiede, B., Urlaub, H., Neubauer, H., Grelle, G., and Wittmann-Liebold, B. (1998) *Biochem. J*. 334, 39−42.
55. Nakagawa, A., Nakashima, T., Taniguchi, M., Hosaka, H., Kimura, M., and Tanaka, I. (1999) *EMBO J*. 18, 1459−1467.
56. Ramakrishnan, V., and White, S. W. (1998) *TIBS* 23, 208−212.
57. Döring, T., Greuer, B., and Brimacombe, R. (1991) *Nucleic Acids Res*. 19, 3517−3524.
58. Stiege, W., Atmadja, J., Zobawa, M., and Brimacombe, R. (1986) *J. Mol. Biol*. 191, 135−138.
59. Wower I., Wower, J. Meinke, M., and Brimacombe, R.(1981) *Nucleic Acids Res* 9, 4285−4302.
60. Wower, J., Hixson, S. S., and Zimmermann, R. A. (1989) *Proc. Natl. Acad. Sci. U.S.A*. 86, 5232−5236.

BI991866O